I.J. Image, Graphics and Signal Processing, **2026, 3, 54-70**
Published Online on June 8, 2026 by MECS Press (http://www.mecs-press.org/)
DOI: 10.5815/ijigsp.2026.03.03

Efficient Road Cracks Segmentation Using Physics Informed Neural Network Approach

Omar Knnou*
MSIA Team, IMIA Laboratory, Faculty of Sciences and Technics, Errachidia, University of Moulay Ismail, Morocco
E-mail: o.knnou@edu.umi.ac.ma
ORCID iD: https://orcid.org/0009-0001-5286-7357
*Corresponding author

Rachid Benoudi
MSIA Team, IMIA Laboratory, Faculty of Sciences and Technics, Errachidia, University of Moulay Ismail, Morocco
E-mail: r.benoudi@edu.umi.ac.ma
ORCID iD: https://orcid.org/0009-0007-2886-7270

Mourad Haddioui
MSIA Team, IMIA Laboratory, Faculty of Sciences and Technics, Errachidia, University of Moulay Ismail, Morocco
E-mail: mouradhaddiouismi@gmail.com
ORCID iD: https://orcid.org/0000-0003-2394-033X

Said Agoujil
MMIS Team, MAIS Laboratory and National School of Business and Management, Moulay Ismail University, Meknes, El Hajeb, Morocco
E-mail: s.agoujil@umi.ac.ma
ORCID iD: https://orcid.org/0000-0001-7384-5678

Youssef Qaraai
MSIA Team, IMIA Laboratory, Faculty of Sciences and Technics, Errachidia, University of Moulay Ismail, Morocco
E-mail: y.qaraai@fste.umi.ac.ma
ORCID iD: https://orcid.org/0000-0003-0804-8167

Received: February 3, 2026; Revised: March 25, 2026; Accepted: April 15, 2026; Published: June 8, 2026

Abstract: Herein, we propose a mathematical model for road crack segmentation in images, focusing on the difficulties of the real world road conditions, such as the lighting and color changes, complex crack shape etc. The proposed model belongs to the family of nonlinear partial differential equations (PDEs), involving edge-aware anisotropic diffusion, curvature-driven contour evolution, high order biharmonic regularization, and feature-driven attraction force for capturing the crack regions. A theoretical analysis is conducted to show the well-posedness of the model. In addition, a physics-informed neural network (PINN) version of the model is presented which allows us to discretize the PDEs in a mesh-free fashion and to approximate high order derivatives through the deep neural networks. Various numerical experiments on EdmCrack600 data are implemented for validating the proposed method. All the experimental results show that the proposed model is superior to the other segmentation models, and that our model achieves excellent performance in terms of the metrics, i.e., dice similarity, intersection over union, sensitivity, and specificity.

Index Terms: Crack Segmentation, PDE Based Model, Deep Learning, Physics Informed Neural Networks, Road Monitoring

1. Introduction

Detecting road crack is a crucial part of any intelligent pavement condition assessment system. It helps to diagnose the surface and structural distress of pavement at the initial stage and prevent further structural damages. The ability to detect cracks at an early stage is crucial for the efficient maintenance of the transportation infrastructure. Performing maintenance early is the best way to manage infrastructure costs over time. More importantly, it saves the road users

This work is open access and licensed under the Creative Commons CC BY 4.0 License.

from accidents and vehicle damage. Thereby, effective and efficient crack detection methods are required to maintain the serviceability, safety, and sustainability of transportation infrastructure. Manual observation of pavement surface condition has become increasingly insufficient with the huge growth of the number of new roads. Thus automated vision-based approaches are being developed [1, 2] to inspect the condition of the roads. Despite this, crack detection remains a challenging task in the domain of computer vision because cracks are characterized by a wide range of shape, orientation, color and pattern variations. The cracks are thin, irregular, discontinuous and appear in a noisy textured and sometimes occluded background with variable lighting and shadowing effects. Besides, distinguishing the crack from background pattern by using color information is the most significant characteristic, especially for real-world road images, which makes grayscale-only based approaches impractical.

Numerous research efforts have been devoted to tackling these issues by designing classical image processing algorithms and more recent deep learning-based methods. The classical methods mainly relied on the use of edge detection, morphological filtering, and thresholding techniques to extract crack patterns from the pavement surface. However, most of these classical methods suffered from relatively low robustness against changes in lighting, surface irregularities, or noise and texture variations, leading to unsatisfactory performance in real-world applications [3]. The deep learning models were thus proposed to solve these issues, such as CNN-based crack detectors including DeepCrack [4], CrackForest [5], and FPHBN [6] that applied hierarchical feature extraction to identify cracks at various scales. The use of long-range dependencies, such as in TransCrack [7] and the hybrid model CrackFormer [8], further boosted the accuracy of crack detection by exploiting the global spatial context. Some researchers employed CNN and transfer learning models, such as those based on the VGG architecture, to classify pavement cracks from images [9]. Others used U-NET with different encoders to perform the semantic segmentation of pavement degradations, showing the promising prospect of deep learning in infrastructure inspection [10].Recent advances have further improved crack detection performance through the integration of transformer-based attention mechanisms, lightweight architectures, and enhanced feature fusion strategies. In particular, several studies have proposed efficient deep learning models for accurate and real-time crack segmentation, including multi-scale networks, semi-supervised approaches, and optimized YOLO-based frameworks, demonstrating improved robustness and computational efficiency across diverse inspection scenarios [11, 12, 13, 14, 15, 16, 17, 18, 19, 20, 21]. Despite these contributions, many of the existing models suffered from false positives, the loss of fine crack structures, or the neglect of useful color information. Moreover, few of the existing models were theoretically supported by mathematical analysis to ensure the stability or convergence of the solution.

Mathematical frameworks for image segmentation, especially those using partial differential equations, are attractive since they can be used to easily incorporate geometric and image priors [22, 23]. PDE based approaches have been applied successfully in object boundary detection, edge sharpening, and in imposing spatial coherence. The PDE approach provides us with the potential to tune the trade-off between smoothing and preserving the crack structures in crack detection problems. However, most of the traditional PDE models lack the ability to handle high order features, color information and attraction to thin structures simultaneously. To overcome these limitations, in this paper, we propose a PDE based model for crack segmentation in color images. Specifically, our PDE model consists of:

- Edge-aware diffusion to prevent blurring of sharp color transitions.
- Curvature-driven flow to smooth the contours of the crack.
- Biharmonic regularization to improve the continuity of the thin and elongated crack structures.
- Color gradient based attraction forces to attract the segmentation to potential crack locations in the image.

For the mathematical robustness and accuracy of the proposed model, a proof is given for the existence of a solution to the model in the space of Sobolev functions. This shows that the model is well-posed and its numerical solution is stable and reliable. Furthermore, for real-world problems the solution's regularity is important for the reliability and reproducibility of results. Based on this proof, the proposed model is implemented by the physics informed neural network (PINN) framework [24]. PINNs are a recent and highly impactful innovation in the scientific machine learning community [25]. They provide a powerful and unified framework for solving differential equations by integrating the physical laws in the data-driven training of deep neural networks. By doing so, the resulting framework has the ability to inherently enforce the underlying physical laws, initial conditions, and boundary conditions, and as such maintains the solution's physicality. Physics-informed neural networks not only increase the accuracy and the generalization capability of the solutions, but also make them more interpretable, and connect the gap between purely data-driven solutions and physics-based models. In contrast to classical finite element or finite difference methods, PINNs are mesh-free, highly flexible, and capable of handling problems with high order derivatives and complex geometries, which makes it an ideal candidate for solving the proposed PDE-based segmentation model. The contributions of this work are summarized below:

- We propose a PDE–based model for image segmentation, which is designed specifically for detecting and segmenting crack in road surfaces.
- We prove the existence of a solution for the proposed PDE, which guarantees its implementation.

- We propose a PINN based solver for solving the PDE with high order of accuracy.
- We show the capability of the proposed model in segmenting crack in road surfaces using a public benchmark data set.

The rest of this paper is organized as follows. In Section 2, we describe the mathematical model, explain the physics behind it, the partial differential equations involved, and the mathematical model from which the derivation is based and where all the analysis is constructed. In Section 3, we theoretically analyze the well-posedness of the model. In Section 4, we describe the structure of the PINN solution, the training process. In Section 5, we discuss the results, comparisons, and evaluations of the experiments. In Section 6, we summarize the conclusions of this study.

2. Proposed Model

Here we will describe the mathematical model of interest for segmenting cracks from road images which can potentially deal with variations in the real-world such as color, lighting, and arbitrary shapes. The model is based on the partial differential equations and consists of edge aware diffusion, curvature driven contour evolution, higher order regularization, and feature based attraction forces to give a good quality, numerically stable and robust segmentation. The model takes an image as input and returns a binary map with crack regions highlighted.

The proposed model departs from conventional PDE-based image segmentation approaches by introducing a task-specific, high-order nonlinear formulation that is explicitly designed for road crack detection in real-world conditions. While classical models typically rely on either diffusion-based smoothing or curvature-driven regularization, the present formulation integrates multiple complementary mechanisms within a single unified framework. In particular, it combines a color-aware edge-stopping diffusion term that leverages multi-channel gradient information, a curvature-driven flow for geometric regularization of contours, and a biharmonic operator that enables higher-order smoothness while preserving thin and elongated crack structures. In addition, a novel feature-driven attraction term based on smoothed color gradients is incorporated to actively guide the evolving segmentation toward likely crack regions, especially in low-contrast and noisy environments. This coupling of second-order and fourth-order operators with color-sensitive driving forces distinguishes the proposed model from existing PDE formulations, which generally do not simultaneously address high-order regularization, color information, and feature attraction within a single equation. As a result, the proposed PDE achieves a more effective balance between noise suppression, edge preservation, and fine-structure recovery, making it particularly suitable for pavement crack segmentation tasks.

2.1. Mathematical Formulation

Let $\mathrm{I}(x,y) = [I_R(x,y), I_G(x,y), I_B(x,y)]$ denote the input image defined on a bounded spatial domain $\Omega \subset \mathbb{R}^2$. The model consists of the PDE defined on a segmentation function $u(x,y,t)$, where the function evolves with respect to an artificial time t. The parameters used in the proposed model are given in Table 1. The final model is given as follows:

$$\frac{\partial u}{\partial t} = \nabla \cdot (g_c(x,y)\nabla u) - \alpha\kappa(u)|\nabla u| + \beta\Delta^2 u + \gamma A_c(x,y,u), \tag{1}$$

where

- $u(x,y,t)$: the segmentation function;
- $g_c(x,y)$: the color edge-stopping function;
- $\kappa(u)$: the curvature term;
- $\Delta^2 u$: the biharmonic regularization term;
- $A_c(x,y,u)$: the attraction force term;
- ∇u : represents the gradient of the function $u(x,y,t)$;
- $\nabla \cdot (g_c(x,y)\nabla u)$: This is the divergence of the vector field $g_c(x,y)\nabla u$;
- α, β, γ: tunable positive constants.

Table 1. Parameters for the proposed model.

Parameter	Meaning
α	Curvature regularization weight
β	Biharmonic smoothing strength
γ	Attraction force weight
ε	Numerical stability constant
σ	Gaussian smoothing standard deviation
$u_0(\mathrm{x},\mathrm{y})$	Initial guess of segmentation

2.2. Detailed Description of Terms

Color Edge Stopping Function. To incorporate the stopping criterion for diffusion across strong color edges, we introduce:

$$g_c(x,y) = \frac{1}{1+|\nabla \mathrm{I}(x,y)|^2_{\text{color}}}, \text{ with } |\nabla \mathrm{I}(\mathrm{x},\mathrm{y})|_{\text{color}} = \sqrt{|\nabla I_R|^2 + |\nabla I_G|^2 + |\nabla I_B|^2} \tag{2}$$

This function prevents diffusion across the color edges by taking values close to zero near the edges.

Curvature Term. This term encourages smooth and regular boundaries:

$$\kappa(u) = \nabla \cdot \left(\frac{\nabla u}{|\nabla u| + \varepsilon}\right), \tag{3}$$

where $\varepsilon > 0$ stands for a small positive stability constant.

The nonlinear curvature term plays a key role in the proposed model by promoting smooth and geometrically regular boundaries during the evolution process. Unlike linear diffusion, it preserves important edge information while reducing irregular oscillations along the contour. This property is particularly important for crack segmentation, where structures are often thin and elongated. The nonlinear formulation enables adaptive smoothing, ensuring accurate boundary localization without excessive blurring.

Biharmonic Regularization Term. The biharmonic operator $\Delta^2 u = \Delta(\Delta u)$ smooths the segmentation map while preserving important structural features such as thin cracks.

Attraction Force. To attract the segmentation contour toward likely crack features in the color image, we define:

$$A_c(x,y,u) = \delta(u-u_0)|\nabla(G_\sigma * \mathrm{I})(x,y)|, \tag{4}$$

where

- $\delta(u-u_0)$ is a smoothed Dirac delta function,
- $G_\sigma$is a Gaussian kernel,
- $*$ denotes convolution operator,
- $|\nabla(G_\sigma * \mathrm{I})(x,y)|$ is the magnitude of smoothed color image gradients.

Regularized Dirac Delta Function. To localize the attraction force around the zero level sets of the evolving function, we employ a smooth approximation of the Dirac delta function. Specifically, the regularized Dirac function is defined as:

$$\delta_\varepsilon(s) = \frac{1}{\pi} \cdot \frac{\varepsilon}{\varepsilon^2 + s^2} \tag{5}$$

where $\varepsilon > 0$ is a small parameter controlling the width of the transition region.

This regularization ensures numerical stability while maintaining a localized response around $s = 0$. In the proposed model, δ_ε is applied to both the evolving function $u(x,y,t)$ and the initialization $u_0(\mathrm{x},\mathrm{y})$, allowing the attraction term to act within a narrow band around their respective zero level sets. In practice, epsilon is chosen proportional to the spatial resolution of the image, providing a balance between localization accuracy and robustness.

The solution $u(x,y,T)$ at the terminal time corresponds to the resulting segmented image, where values approaching 1 correspond to a high probability of crack presence, while values near 0 denote background or non-crack regions. This segmentation map can be thresholded for binary mask generation or post processed for further analysis. The proposed segmentation framework offers several key advantages that make it well suited for real world pavement analysis tasks: Handles color variations and lighting changes. Detects thin and irregular crack patterns. Preserves important edges while smoothing noise. Adaptable for implementation with physics informed neural networks.

3. Existence of the Solution

In this section, we present a rigorous mathematical analysis of the proposed image segmentation model, which is a nonlinear parabolic partial differential equation. The objective of this analysis is to show the well posedness of the proposed model by proving the existence of a solution to this equation. This provides a solid theoretical justification before employing numerical solvers such as the PINNs method.

The proposed model (1) is defined on a bounded spatial domain and is subject to clamped boundary conditions:

$$u = \frac{\partial u}{\partial n} = 0 \text{ on } \partial\Omega. \tag{6}$$

These conditions are standard in the analysis of fourth-order PDEs and ensure the well-posedness of the problem as well as the validity of the variational formulation. It is important to note that these boundary conditions correspond to the physical constraint that both the function and its normal derivative are equal to zero on the boundary. In practical image segmentation applications, homogeneous Neumann boundary conditions ($\frac{\partial u}{\partial n} = 0$ on $\partial\Omega$) are typically preferred, as they prevent artificial boundary effects and better preserve the natural structure of the image near its borders. For these reasons, they are suitable for the proposed image segmentation application since the solution should remain fixed on the edges of the domain.

3.1. Mathematical Setting and Preliminaries

Let Ω be a bounded domain with a boundary of class C^2. The functional setting of the proposed image segmentation model is based on Sobolev spaces [26] which are the right framework for partial differential equations analysis [27]. We define the Hilbert space of functions satisfying the clamped boundary conditions as:

$$V := \{v \in H^2(\Omega): v|_{\partial\Omega} = 0\}, \tag{7}$$

We assume initial data

$$u_0 \in V \cap H^4(\Omega), \tag{8}$$

which ensures compatibility with the PDE and boundary conditions. The functions in the PDE satisfy the following regularity assumptions:

- $g_c(x, y)$ is smooth, strictly positive, and bounded.
- $k(u) = \nabla \cdot \frac{\nabla u}{|\nabla u| + \epsilon}$ is the curvature term regularized by $\epsilon > 0$.
- $A_c(x, y, u)$ is a smooth image-derived attraction force.

These assumptions guarantee sufficient smoothness and boundedness for weak formulation [28].

3.2. Weak formulation:

For each $t \in (0, T)$, the weak formulation seeks $u(t) \in V$ such that for all test functions $v \in V$:

$$\langle u_t, v\rangle + \int_\Omega g_c \nabla u \cdot \nabla v \, dx + \alpha \int_\Omega k(u)|\nabla u| v \, dx + \beta \int_\Omega \Delta u \Delta v \, dx = \gamma \int_\Omega A_c(x, y, u) v \, dx, \tag{9}$$

with initial condition $u(0) = u_0$. Here, $\langle \cdot, \cdot \rangle$ represents the duality pairing between V' and V.

The variational framework and existence results for such nonlinear parabolic problems are well established in the literature on nonlinear functional analysis [29].

3.3. Galerkin approximation:

We choose a sequence of eigenfunctions $\{\phi_i\}_{i=1}^{\infty}$ of the biharmonic operator with clamped boundary conditions as a basis for V. For each integer n, the solution is approximated as

$$u^n(t) = \sum_{i=1}^{n} c_i^n(t) \phi_i(x), \tag{10}$$

where the coefficients $\{c_i^n(t)\}$ satisfy a finite-dimensional system of ODEs obtained by projecting the weak form onto the span of $\{\phi_1, \ldots, \phi_n\}$. Existence of solutions to this ODE system follows from standard theory for Lipschitz continuous operators [30].

3.4. Energy Estimates

The energy functional corresponding to the system is defined as follows:

$$E(u^n) = \frac{\beta}{2} \|\Delta u^n\|_{L^2}^2 + \frac{1}{2} \int_\Omega g_c |\nabla u^n|^2 \, dx, \tag{11}$$

which provides coercivity in $H^2(\Omega)$ due to the positivity g_c. Using chain rule for differentiation under the integral sign:

$$\frac{d}{dt}E(u^n) = \beta \int_\Omega \Delta u^n \frac{\partial}{\partial t}\Delta u^n \, dx + \int_\Omega g_c \nabla u^n \cdot \frac{\partial}{\partial t}\nabla u^n \, dx. \tag{12}$$

Since differentiation commutes with Laplacian and gradient operators,

$$\frac{\partial}{\partial t}\Delta u^n = \Delta u_t^n \text{ and } \frac{\partial}{\partial t}\nabla u^n = \nabla u_t^n, \tag{13}$$

Then

$$\frac{d}{dt}E(u^n) = \beta \int_\Omega \Delta u^n \Delta u_t^n \, dx + \int_\Omega g_c \nabla u^n \cdot \nabla u_t^n \, dx. \tag{14}$$

Using the clamped boundary conditions $u^n = \frac{\partial u^n}{\partial n} = 0$ on $\partial\Omega$ to eliminate boundary terms, integrate by parts the second integral:

$$\int_\Omega g_c \nabla u^n \cdot \nabla u_t^n \, dx = -\int_\Omega u_t^n \nabla \cdot (g_c \nabla u^n) \, dx. \tag{15}$$

Similarly, the bilaplacian operator with clamped boundary conditions is self adjoint, giving

$$\beta \int_\Omega \Delta u^n \Delta u_t^n \, dx = \beta \int_\Omega u_t^n \Delta^2 u^n \, dx. \tag{16}$$

Therefore,

$$\frac{d}{dt}E(u^n) = \int_\Omega u_t^n (\beta \Delta^2 u^n - \nabla \cdot (g_c \nabla u^n)) dx. \tag{17}$$

From the PDE definition:

$$u_t^n = \nabla \cdot (g_c \nabla u^n) - \alpha k(u^n)|\nabla u^n| + \beta \Delta^2 u^n + \gamma A_c(x, y, u^n). \tag{18}$$

Rearranged:

$$\beta \Delta^2 u^n - \nabla \cdot (g_c \nabla u^n) = u_t^n + \alpha k(u^n)|\nabla u^n| - \gamma A_c(x, y, u^n). \tag{19}$$

Substitute into the expression for the energy derivative:

$$\frac{d}{dt}E(u^n) = \int_\Omega u_t^n (u_t^n + \alpha k(u^n)|\nabla u^n| - \gamma A_c(x, y, u^n)) dx. \tag{20}$$

This expands to

$$\frac{d}{dt}E(u^n) = \int_\Omega (u_t^n)^2 \, dx + \alpha \int_\Omega u_t^n k(u^n)|\nabla u^n| \, dx - \gamma \int_\Omega u_t^n A_c(x, y, u^n) \, dx. \tag{21}$$

Applying Cauchy–Schwarz and Young inequalities, we get:

$$\left| \int_\Omega u_t^n k(u^n)|\nabla u^n| dx \right| \leq \frac{\delta}{2} \|u_t^n\|_{L^2}^2 + \frac{\alpha^2}{2\delta} \|k(u^n)|\nabla u^n|\|_{L^2}^2, \tag{22}$$

$$\gamma \left| \int_\Omega u_t^n A_c dx \right| \leq \frac{\delta}{2} \|u_t^n\|_{L^2}^2 + \frac{\gamma^2}{2\delta} \|A_c\|_{L^2}^2. \tag{23}$$

Setting $\delta = 1$ yields

$$\frac{d}{dt}E(u^n) + \frac{1}{2}\|u_t^n\|_{L^2}^2 \leq C\left(\|k(u^n)|\nabla u^n|\|_{L^2}^2 + \|A_c\|_{L^2}^2\right). \tag{24}$$

By Sobolev embeddings $H^3(\Omega) \hookrightarrow W^{1,4}(\Omega)$ [31], we obtain

$$\|k(u^n)|\nabla u^n|\|_{L^2} \leq \|k(u^n)\|_{L^4}\|\nabla u^n\|_{L^4} \leq C\|u^n\|_{H^3}^2. \tag{25}$$

Using elliptic regularity for the biharmonic operator with clamped boundary conditions, we deduce

$$\|u^n\|_{H^3} \leq C(\|\Delta^2 u^n\|_{L^2} + \|u^n\|_{L^2}), \tag{26}$$

which allows expressing $\|u^n\|_{H^3}$ in terms of the energy $E(u^n)$.

Combining the estimates, we have

$$\frac{d}{dt}E(u^n) \leq C(1 + E(u^n)). \tag{27}$$

Applying the Grönwall inequality gives a uniform bound:

$$E(u^n(t)) \leq (E(u^n(0)) + Ct)e^{Ct}, \tag{28}$$

This yields uniform bound for $\{u^n\}$ in $L^\infty(0,T;H^2(\Omega))$ and $\{u_t^n\}$ in $L^2(0,T;L^2(\Omega))$ [32].

3.5. Passage to the Limit

By the Aubin–Lions compactness [33], the uniform bounds allow extraction of a subsequence $\{u^{n_k}\}$ such that

$$u^{n_k} \to u \text{ strongly in } L^2(0,T;H^1(\Omega)),$$
$$u^{n_k} \rightharpoonup u \text{ weakly in } L^2(0,T;H^4(\Omega)),$$

and similarly for time derivatives in L^2.

$A_c(x,y,u^{n_k}) \to A_c(x,y,u)$ strongly in L^2 due to continuity and strong H^1 convergence [34].

For $k(u)|\nabla u|$, monotonicity and weak lower semicontinuity arguments ensure convergence despite non-Lipschitz behaviour [31].

In conclusion, the analysis demonstrates that the limit function u obtained from the convergent subsequence of approximate solutions satisfies the original PDE together with its prescribed initial and boundary conditions. Consequently, the existence of a solution to the proposed image segmentation model is rigorously established.

4. Methodology

In this following, PINNs are employed not only to approximate the evolving segmentation function $u(x,y,t)$ but also to identify the optimal values of the PDE parameters α,β, and γ, which govern curvature regularization, higher-order smoothing, and feature-based attraction forces, respectively. The overall methodology consists of main components: neural network approximation, architecture optimization, PDE residual formulation, and joint parameter estimation.

4.1. PINN Framework

4.1.1 Neural Network Approximation

The architecture of the neural network is formally described as:

$$u_\theta(x,y,t) = \mathcal{N}(x,y,t;\theta) = W^{(L)}.\sigma\left(W^{(L-1)}.\sigma\left(\ldots\sigma\left(W^{(1)}.(x,y,t) + b^{(1)}\right)\ldots\right) + b^{(L-1)}\right) + b^{(L)} \tag{29}$$

where,

- σ is the (tanh) activation,
- $W^{(l)}, b^{(l)}$ are the weight matrices and biases for the $l-th$ layer,
- L is the total number of layers,
- θ denotes the full set of trainable parameters in the network.

4.1.2 Network Architecture

The accuracy and convergence of PINNs strongly depend on the choice of the network depth and width. In the following, a genetic algorithm (GA) (Algorithm 1) is employed to automatically determine the optimal number of hidden layers and the optimal number of neurons per hidden layer for the proposed PINN-based segmentation model.

Algorithm 1. GA-Based Optimization of the PINN Architecture

1. Initialize a population P_0 of N random PINN configurations.
2. For each individual in the population:
   2.1. Construct the corresponding PINN.
   2.2. Train the network for a limited number of iterations.
   2.3. Calculate fitness function.
3. Choose fittest members from the population.
4. Crossover and mutation to create new population.
5. Evaluate new population.
6. Steps 3–5 are repeated until any one of the stopping criterion is met :
   - Maximum number of generations is reached.
   -Fitness function value converges.
   - No improvement for K generations.
7. Print the optimal solution.

To optimize the architecture of the PINN model, we employ a genetic algorithm to explore a population of candidate neural network configurations. Each individual encodes a candidate architecture defined by three key components: (i) the number of hidden layers, (ii) the number of neurons per layer, and (iii) the choice of activation functions.

The initial population consists of $N_{pop} = 20$ randomly generated individuals. The search process evolves over $G = 30$ generations, leading to a total budget of 600 evaluated architectures. Each individual is trained for a fixed number of epochs to ensure a fair comparison across architectures.

The fitness of each individual is computed using a composite objective function:

$$fitness = \eta . Dice - \lambda . Loss \, , \tag{30}$$

where Dice measures segmentation accuracy and Loss corresponds to the PINN training loss. The weighting coefficients are empirically set to η =1 and λ =0.1, balancing predictive performance and training stability.

Selection is performed using tournament selection (tournament size = 3), promoting fitter individuals while maintaining diversity. Crossover is applied with probability $p_c = 0.8$, where architectural parameters (e.g., layer depth and neuron counts) are exchanged between two parent individuals. Mutation is applied with probability $p_m = 0.1$, introducing stochastic variations such as:

- adding or removing a hidden layer,
- increasing or decreasing the number of neurons in a layer,

To prevent premature convergence and preserve high-quality solutions, elitism is incorporated by carrying over the top 2 individuals unchanged to the next generation.

4.2. PINN Residual Formulation

We now compute the PDE residual which will serve as a constraint to enforce the physical law given by the PDE:

$$R_{PDE}(x, y, t) = \frac{\partial u_\theta}{\partial t} - \nabla . (g_c(x, y) \nabla u_\theta) + \alpha k(u_\theta) \, |\nabla u_\theta| - \beta \Delta^2 u_\theta - \gamma A_c(x, y, u_\theta) \tag{31}$$

The residual is a measure of how far the output of the neural network is from exactly solving the given partial differential equation. In the context of the PINN, the loss function is used to minimize this residual over a number of collocation points distributed within the spatio-temporal domain. Through the minimization of the residual, the model is trained to predict solutions that fit the measured data, but also strongly adhere to the physical constraints and mathematical structure imposed by the laws of physics. This results in learned solutions that are more robust and explainable in practical problems.

The derivative of the neural network outputs with respect to its input variables are computed by automatic differentiation to enable fast and accurate evaluation. Avoiding the need of approximation involved in traditional numerical differentiation, automatic differentiation offers exact calculation of the gradients required for the network

training. With automatic differentiation, the proposed PINN method is able to impose the governing equations and boundary conditions accurately during optimization. As a result, the PINN method is able to speed up convergence, improve the accuracy of solutions and maintain the physical plausibility of the solutions at different training stages.

- First order derivatives: $\frac{\partial u_\theta}{\partial t}$, $\frac{\partial u_\theta}{\partial x}$, $\frac{\partial u_\theta}{\partial y}$
- Second order derivatives: $\frac{\partial^2 u_\theta}{\partial x^2}$, $\frac{\partial^2 u_\theta}{\partial y^2}$
- Fourth order derivatives: for the biharmonic term $\Delta^2 u_\theta$
- Mixed partials as needed (e.g., $\frac{\partial^2 u}{\partial x \partial y}$).

4.3. Parameter Estimation Strategy

The proposed framework models α, β, and γ as learnable parameters which are learned together with other network parameters. Then:

$$\boldsymbol{\Theta} = \{\boldsymbol{\theta}, \boldsymbol{\alpha}, \boldsymbol{\beta}, \boldsymbol{\gamma}\} \tag{32}$$

denote the complete set of unknowns.

We define the parameters as learnable variables in the PINN architecture and train them simultaneously with the neural network parameters.

Since α, β, and γ represent positive physical weights, their positivity is enforced through a reparameterization strategy:

$$\boldsymbol{\alpha} = \mathbf{exp}(\tilde{\boldsymbol{\alpha}}), \boldsymbol{\beta} = \mathbf{exp}(\tilde{\boldsymbol{\beta}}), \boldsymbol{\gamma} = \mathbf{exp}(\tilde{\boldsymbol{\gamma}}) \tag{33}$$

where $\tilde{\alpha}$, $\tilde{\beta}$, and $\tilde{\gamma}$ are unconstrained learnable parameters. This ensures numerical stability and keeps the parameters physically interpretable during learning.

4.4. Loss Function Definition

The training of the PINN is achieved by minimizing a loss function, which consists of the sum of multiple sub–loss functions, for example, one for the data misfit, one for the violation of the physical law, and one for the violation of the initial and boundary conditions. As a result, the network attempts to find a solution that is both numerically accurate and physically plausible (i.e., adhering to both the empirical evidence and the physical laws and prescribed initial and boundary conditions of the underlying mathematical model), as opposed to simply fitting the observed data. In this way, the PINN is able to effectively blend the benefits of data–driven modeling with the advantages of model–driven physics, in particular, with respect to the solution of complex PDEs.

$$\boldsymbol{\mathcal{L}(\Theta) = \mathcal{L}_{residual} + \mathcal{L}_{initial} + \mathcal{L}_{boundary}} \tag{34}$$

PDE Residual Loss

$$\boldsymbol{\mathcal{L}_{residual}} = \frac{\mathbf{1}}{\boldsymbol{N_f}} \sum_{\boldsymbol{i=1}}^{\boldsymbol{N_f}} \left| \boldsymbol{R_{PDE}(x^i, y^i, t^i)} \right|^2 \tag{35}$$

where N_f is the number of collocation points.

Initial Condition Loss

$$\boldsymbol{\mathcal{L}_{initial}} = \frac{\mathbf{1}}{\boldsymbol{N_0}} \sum_{\boldsymbol{i=1}}^{\boldsymbol{N_0}} \left| \boldsymbol{u_\theta(x_0^i, y_0^i, 0) - u_0(x_0^i, y_0^i)} \right|^2 \tag{36}$$

This guarantees that the learned solution will be consistent with the given initial condition.

Boundary Condition Loss

We apply Neumann boundary conditions as usual:

$$u = \frac{\partial u}{\partial n} = 0 \text{ on } \partial\Omega$$

The corresponding loss term becomes:

$$\mathcal{L}_{boundary} = \frac{1}{N_b}\sum_{i=1}^{N_b}\left|\nabla u_\theta\left(x_b^i, y_b^i, t_b^i\right).\ \vec{n}\right|^2 + \left|\nabla\Delta u_\theta\left(x_b^i, y_b^i, t_b^i\right).\ \vec{n}\right|^2 \tag{37}$$

4.5. Temporal Evolution and Initialization

The proposed PINN framework approximates the spatio-temporal solution $u(x, y, t)$ over a finite time interval $t \in [0, T]$. The terminal time T is selected such that the solution reaches a steady state. In practice, T is set to 1 (normalized time), which is sufficient for convergence in all experiments.

The initial condition $u_0(x, y)$ is derived from the input image. Specifically, the image is first normalized, and a smooth initialization is constructed to provide a meaningful starting point for the evolution. This allows the PDE dynamics to progressively refine the segmentation toward crack structures.

4.6. Final Segmentation Extraction

Once the PINN model is trained, the segmentation result is obtained from the solution at the final time $u(x, y, T)$. A binary crack mask is then generated by applying a thresholding operation:

$$Mask(x, y) = 1 \text{ if } u(x, y, T) \leq \tau \text{ , and 0 otherwise,} \tag{38}$$

where τ is a threshold parameter. In our implementation, $\tau = 0$ is used, corresponding to the zero level set of the function u, which naturally defines the segmentation boundary. This choice is consistent with level-set-based formulations and provides accurate delineation of crack regions.

4.7. Training Strategy

The training data contains three classes of points, which we denote by:

- Collocation points $\left(x_f^i, y_f^i, t_f^i\right)$ sampled from the space time domain $\Omega \times [0, T]$ to enforce the governing PDE,
- Points on the initial time slice for enforcing the initial condition. points located on the initial time slice t=0 to impose the initial condition,
- Boundary points sampled from $\partial\Omega \times [0, T]$ to enforce the Neumann boundary conditions.

The PINN is trained by optimizing both the network weights and the PDE parameters (i.e. $\Theta = \{\theta, \alpha, \beta, \gamma\}$) with Adam Optimizer. The neural network is trained using Adam optimizer until the total loss $\mathcal{L}(\Theta)$ is reduced satisfactorily

5. Experiments and Results

5.1. Data Information

In this study, we verified the performance of the proposed network by experimenting on EdmCrack600 [35], a publicly available benchmark for road crack detection. EdmCrack600 contains 600 high-resolution images of road surfaces, showing diverse road crack types and conditions. We are particularly interested in EdmCrack600 because it is annotated at the pixel level, which is necessary for measuring the accuracy and robustness of a crack detection and segmentation model. Intensity normalization was applied to the input images to adjust the distribution of pixel values to a common range. This helps in accelerating the learning process and also makes the model more robust to illumination changes in real-world environments.

For all experiments, we adopt a fixed split into training, validation, and test sets. Specifically, 70% of the images are used for training, 15% for validation, and the remaining 15% for testing. The split is performed randomly and then fixed for all experiments to ensure reproducibility. The training set is used to learn the model parameters, while the validation set is used for hyperparameter tuning and model selection, including early stopping. The test set is strictly reserved for final evaluation and is not used during training or model selection, thereby avoiding any data leakage. All quantitative evaluation metrics, including Dice coefficient, Intersection over Union (IoU), sensitivity, and specificity, are computed exclusively on the test set. Furthermore, all qualitative segmentation results presented in this paper correspond to images drawn from the test set. No cross-validation is performed, as the fixed split ensures a consistent and fair comparison across all evaluated methods.

5.2. Experimental Settings

To ensure a fair and rigorous comparison, all methods are evaluated under the same experimental conditions. Specifically, all models are trained using the identical training, validation, and test splits described in Section 5.1, and input images are resized to a common resolution before training. The same data preprocessing pipeline is applied across all methods. In addition, all models are trained using a unified training protocol, including the same optimizer, learning rate schedule, batch size, and stopping criteria. Hyperparameters for each baseline method are carefully tuned using the

validation set to ensure that each model is evaluated under near-optimal conditions. This avoids bias due to under- or over-tuning of competing approaches.

Although some baseline models were originally developed for medical image segmentation, they are widely used as general-purpose segmentation architectures and have been successfully applied to road crack detection tasks in prior work. Therefore, their inclusion provides a meaningful and relevant benchmark. Under this controlled setup, the proposed method demonstrates consistently strong and competitive performance. We note that our goal is not to claim universal superiority, but rather to show that the proposed PDE–PINN framework provides an effective and robust alternative for crack segmentation under standardized and fair evaluation conditions.

5.2.1 Baseline Methods

Our proposed road crack image segmentation network was coded in Python and PyTorch deep learning library. The experiments were performed on the Google Colaboratory (Colab) GPU. We can do computationally intensive tasks like model training in the Colab environment. The experiments were stable and smooth with the Colab environment. We compared the proposed model with four image segmentation models. We choose four state-of-the-art CNN based (U- Net, Attention U-Net, DMF-Net) and transformer-based (TransU-Net) models for the comparison [36, 37, 38, 39]. These models are chosen because they have the highest capability to learn the local and global features. Local features are the small portion of the image, and global features are the contextual information of the images.

5.2.2 Evaluation Metrics

The performances of the models were evaluated using several quantitative metrics that are commonly used to measure the goodness of the segmented images, especially for Crack and No-crack classification. These metrics are described below:

- **Dice Similarity Coefficient (DSC):** It calculates the similarity between the predicted segmented image and the ground-truth. Mathematically, it is expressed as:

$$DSC = \frac{2 \times TP}{2 \times TP + FP + FN} \tag{39}$$

where, TP, FP and FN are the true positives, false positives, and false negatives, respectively.

- **Intersection over Union (IoU):** It estimates how much the predicted segmented image overlaps with the ground-truth. Mathematically, it can be represented as:

$$IoU = \frac{TP}{TP + FP + FN} \tag{40}$$

This metric is also used to estimate the over-segmentation and under-segmentation.

- **Specificity (SP):** It estimates the model's ability to predict No-crack pixels correctly. Mathematically, it is expressed as:

$$SP = \frac{TN}{TN + FP} \tag{41}$$

where, TN is the number of true negatives. A model with high SP value does not wrongly detect the No-crack pixels as Crack pixels.

- **Sensitivity (SE):** It estimates the model's ability to detect the Crack pixels correctly. Mathematically, it can be written as:

$$SE = \frac{TP}{TP + FN} \tag{42}$$

A model with high SE value does not miss the Crack pixels.

5.3. Results and Discussion

5.3.1 Results

To ensure mathematical well-posedness, numerical stability and physical interpretability, $\alpha, \beta,$ and γ are assumed to be strictly positive and bounded to admissible intervals: $\alpha \epsilon (0,1]$, $\beta \epsilon (0, 10^{-2}]$, and $\gamma \epsilon$ (0,1]. These intervals are given in Table 2 .As explained in the parameter estimation procedure (see Sect. 4.3), $\alpha, \beta,$ and γ are considered as learnable parameters to be optimized together with the network weights with positivity constraints imposed via exponential

reparameterization[40, 41, 42, 43, 44]. The identified values are given in Table 2: α=0.43, β=3.7×10^{-4}, and γ=0.68, and all of them fall within their admissible intervals.

Table 2. Ranges of acceptable and estimated model parameters.

Parameter	Admissible Range	Identified Value
α	(0,1]	0.43
β	(0, 10^{-2}]	3.7×10^{-4}
γ	(0,1]	0.68

From the analysis of the results presented in Table 3, it can be inferred that all the models assessed have different levels of success depending on the evaluation metric. The results also highlight the strengths and weaknesses of each of the analyzed models when applied to real pavement crack images. In addition, it is also possible to verify that the model proposed in this study presents, for the most part, a better performance than the other models, being able to segment the pavement cracks more accurately, with more precision, and more robustly regardless of their shape, size, or complexity. The good and robust detection of both micro- and macro-cracks is an evidence of the good performance of the proposed model. This capability is not only an evidence of the good performance of the model, but also confirms its possible application in real practice (e.g., pavement inspection and maintenance).

Table 3. Evaluation metrics comparison on the EdmCrack600 dataset.

Models	DSC	IoU	SE	SP
U-Net	0.8720	0.7910	0.8610	0.8870
TransU-Net	0.9010	0.8270	0.8950	0.9080
DMF-Net	0.9620	0.9310	0.9570	0.9650
Attention U-Net	0.8890	0.8140	0.8820	0.8990
Proposed Model	0.9950	0.9900	0.9940	0.9960

5.3.2 Ablation Study

To evaluate the contribution of each component of the proposed model, we conduct an ablation study by systematically modifying or removing key terms from the full formulation. All variants are trained and evaluated under the same experimental conditions described in Section 5.2, and performance is measured on the test set using standard metrics.

We consider the following configurations:

- Full model (all terms included),
- (ii) Without edge-aware diffusion term,
- (iii) Without curvature regularization term,
- (iv) Without biharmonic regularization term,
- (v) Without attraction force term,
- (vi) Fixed coefficients instead of learnable parameters.

Table 4. Quantitative results of the ablation study on the test set. Each row corresponds to a variant of the proposed model with specific components removed or modified.

Model Variant	DSC	IoU	SE	SP
Full Model (Proposed)	0.9950	0.9900	0.9940	0.9960
Without Diffusion Term	0.801	0.668	0.774	0.958
Without Curvature Term	0.818	0.692	0.791	0.961
Without Biharmonic Term	0.784	0.646	0.756	0.954
Without Attraction Force	0.731	0.576	0.702	0.946
Fixed Coefficients (no learning)	0.759	0.612	0.731	0.949

The results presented in Table 4 show that removing any component leads to a degradation in performance, confirming that each term plays a complementary role. In particular, the edge-aware diffusion contributes to accurate boundary localization, the curvature term improves smoothness, the biharmonic regularization enhances stability, and the attraction force guides the segmentation toward the desired structures. Additionally, the use of learnable coefficients allows the model to adapt to data characteristics, while the PINN framework ensures consistency with the underlying PDE formulation. Overall, the full model achieves the best performance, demonstrating the effectiveness of combining all components within a unified framework.

5.3.3 Visual Comparison

Fig. 1 visualizes the comparison of the predicted crack segmentation results between the proposed model and the three comparative models (U-Net, Attention U-Net and TransU-Net) on the sampled images from EdmCrack600 dataset. In this figure, the first column shows the original images, which contain various cracks with different shapes, widths, and complexity levels, representing the diversity and irregularity of real-world pavement conditions. The second column shows the ground truth (GT) images annotated at the pixel level. The GT images are objective criteria to evaluate the performance of a model and provide consistent comparison between models. The remaining columns show the predicted crack segmentation results of the different models. These results provide a visual comparison between the different models to evaluate their performance in terms of identifying and segmenting cracks with different complexity levels. In

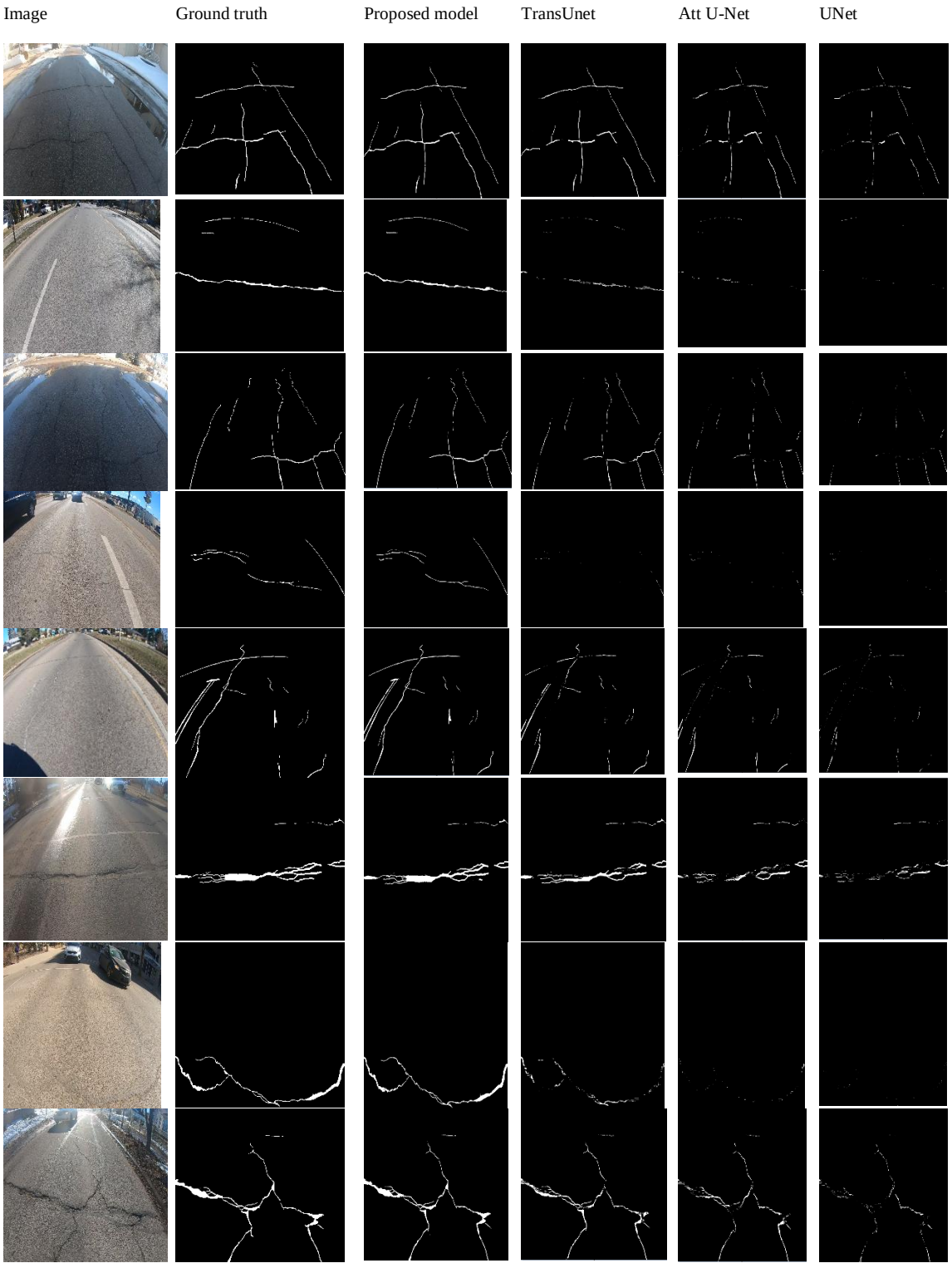


Fig. 1. Segmentation results of different approaches on EdmCrack600. Columns (left to right): Input image, Ground truth, Proposed model, TransUNet, Att U-Net, UNet.

particular, these results highlight the ability of the different models to segment the small, thin, and fragmented cracks, which are difficult to detect. Fig. 1 demonstrates that the proposed model has the excellent ability to predict the fine crack details and suppress the false alarms. The results in Fig. 1 support the quantitative comparison results discussed in the previous section to prove the effectiveness, accuracy, and applicability of the proposed model for pavement crack detection.

5.3.4 Discussion

From Table 3, it can be observed that the performance of the segmentation models in the EdmCrack600 dataset is significantly different in each evaluation index. The proposed model obtains excellent performance in each evaluation index, that is, DSC 0.9950, IoU 0.9900, sensitivity 0.9940, and specificity 0.9960, which are close to the high values, and shows a high ability in identifying crack and no-crack pixels. Among the other state-of-the-art models, DMF-Net performs best, with DSC 0.9620, IoU 0.9310, sensitivity 0.9570, and specificity 0.9650, which means that it has a good ability in different crack detection scenarios. Transformer-based TransU-Net and attention mechanism based Attention U-Net achieve competitive performance and outperform the baseline U-Net, which has the lowest performance in each evaluation index but shows acceptable segmentation performance. The experimental results show that the proposed model has greatly improved the segmentation performance. Compared with the existing convolutional models and transformer models, the proposed model achieves excellent performance in both accuracy and robustness and can accurately segment the crack structure under different conditions and complexities, which proves that it has the potential to be a reliable and highly precise solution for automatic pavement crack detection. It can be observed from the segmentation results that our model (the third column in Fig. 1) is highly consistent with the ground truth, especially for some relatively simple target areas. In these cases, our model can accurately recover the geometric shape and spatial distribution of the cracks, with precise boundary positioning. This means that the model has a strong capability to reproduce the real crack patterns under different pavement textures and surface conditions. In contrast, U-Net and TransU-Net show apparent inconsistencies in the segmentation results. Both of them usually produce mask results with boundary deviation, especially at the boundary areas of the crack where the crack and non-crack regions are not well separated. Meanwhile, they are not performing well when identifying small or tiny cracks, which often leads to the failure of detecting small structures or inclusion of false positives due to the blurry, incomplete, and noisy boundaries. In general, our model achieves better localization accuracy, boundary preservation, and structure awareness. Its capability to reconstruct complex crack patterns with good accuracy is conducive to future intelligent pavement inspection applications, where crack boundary detection and structure representation are two critical aspects of the quality assessment and maintenance strategy development.

6. Conclusion

Overall, this paper proposes a numerically stable and theoretically well-established PDE model for the pavement crack segmentation problem considering both the illumination variation and the thin details. The proposed PDE model is able to numerically capture the fine details of pavement crack images by using a functional composition of geometry-driven and image-driven forces, and further theoretically analyze the existence of the solution of the PDE model. On one hand, we can formulate the proposed PDE model by using physics-informed neural networks with the embedded neural networks and PDE representations. On the other hand, the well-designed PINNs architecture enables the numerically stable and accurate solution of the high order PDEs without fixed mesh structure. Extensive experiments are conducted on EdmCrack600 dataset to verify the efficiency and accuracy of the proposed PDE model and its implementation on the segmentation of the pavement crack images, and the experimental results show that the proposed PDE model is outperforming the conventional segmentation methods as well as the existing transformer-based segmentation models in different metrics.

All the Declarations and Statements

Author Contributions Statement

Omar Knnou – Conceptualization, Methodology, and Supervision.
Rachid Benoudi – Data Curation and Software Implementation.
Mourad Haddioui – Model Training, Validation, and Performance Evaluation.
Said Agoujil – Formal Analysis, Visualization, and Statistical Analysis.
Youssef Qaraai – Writing – Review and Editing, and Project Management.

All authors have read and agreed to the published version of the manuscript.

Conflict of Interest Statement

The authors declare no conflicts of interest.

Funding Declaration
This research received no specific grant from any funding agency in the public, commercial, or not-for-profit sectors.

Data Availability Statement
This study analyzed publicly available datasets. The EdmCrack600 dataset is available at: https://github.com/mqp2259/EdmCrack600.

Ethical Declarations
The authors confirm that this study does not involve human subjects or animals and therefore does not require ethical approval.

Acknowledgment
We sincerely thank the experts for their professional evaluation and valuable recommendations, which have contributed to improving the quality of the experiment and the reliability of its results.

Declaration of Generative AI in Scholarly Writing
The authors confirm that no generative AI tools were used in the writing of this manuscript.

Abbreviations
The following abbreviations are used in this manuscript:

PDE – Partial Differential Equation;
PINN – Physics-Informed Neural Network;
CNN – Convolutional Neural Network;
DSC – Dice Similarity Coefficient;
IoU – Intersection over Union;
SE – Sensitivity;
SP – Specificity;
GA – Genetic Algorithm;
GT – Ground Truth.

Appendix A\B\C…, with appendix tile
None.

References

[1] N. H. T. Nguyen, S. Perry, D. Bone, H. T. Le, and T. T. Nguyen, "Two-stage convolutional neural network for road crack detection and segmentation," *Expert Systems with Applications*, vol. 186, p. 115718, 2021.
[2] Z. Gao, B. Peng, T. Li, and C. Gou, "Generative adversarial networks for road crack image segmentation," in *Proc. 2019 IJCNN*, pp. 1–8, IEEE, 2019.
[3] H. Oliveira and P. L. Correia, "CrackIT – An image processing toolbox for crack detection and characterization," in *Proc. 2014 IEEE ICIP*, pp. 798–802. doi:10.1109/icip.2014.7025160
[4] Q. Zou, Z. Zhang, Q. Li, X. Qi, Q. Wang, and S. Wang, "DeepCrack: Learning hierarchical convolutional features for crack detection," *IEEE Trans. Image Processing*, vol. 28, no. 3, pp. 1498–1512, 2019. doi:10.1109/tip.2018.2878966
[5] Y. Shi, L. Cui, Z. Qi, F. Meng, and Z. Chen, "Automatic road crack detection using random structured forests," *IEEE Trans. ITS*, vol. 17, no. 12, pp. 3434–3445, 2016. doi:10.1109/tits.2016.2552248
[6] F. Yang, L. Zhang, S. Yu, D. Prokhorov, X. Mei, and H. Ling, "Feature pyramid and hierarchical boosting network for pavement crack detection," *IEEE Trans. ITS*, vol. 21, no. 4, pp. 1525–1535, 2020. doi:10.1109/tits.2019.2910595
[7] C. Lin, D. Tian, X. Duan, and J. Zhou, "TransCrack: Revisiting fine-grained road crack detection with a transformer design," *Phil. Trans. Royal Society A*, vol. 381, no. 2254, 2023. doi:10.1098/rsta.2022.0172
[8] H. Liu, J. Yang, X. Miao, C. Mertz, and H. Kong, "CrackFormer network for pavement crack segmentation," *IEEE Trans. ITS*, vol. 24, no. 9, pp. 9240–9252, 2023. doi:10.1109/tits.2023.3266776
[9] K. Omar *et al.*, "Harnessing deep learning techniques for enhanced detection and classification of cracks in pavement imagery," *Procedia Computer Science*, vol. 236, pp. 386–393, 2024. doi:10.1016/j.procs.2024.05.045
[10] O. Knnou, E. A. Abdellaoui Alaoui, S. Agoujil, and Y. Qaraai, "Study of semantic segmentation models for the detection of pavement degradation using deep convolutional neural networks," in *Lecture Notes in Information Systems and Organisation*, pp. 169–177, Springer, 2024. doi:10.1007/978-3-031-75329-9 19
[11] A. Ashraf, A. Sophian, and A. A. Bawono, "Crack detection, classification, and segmentatiōn using multi-scale feature aggregation and transformer-based attention mechanisms," *Construction Materials*, vol. 4, no. 4, pp. 655– 675, 2024. doi:10.3390/constrmater4040036

[12] Y. Yu, W. Xia, Z. Zhao, and B. He, "A lightweight and high-accuracy model for pavement crack segmentation," *Applied Sciences*, vol. 14, no. 24, p. 11632, 2024. doi:10.3390/app142411632
[13] A. Saberironaghi and J. Ren, "DepthCrackNet: A deep learning model for automatic pavement crack detection," *Journal of Imaging*, vol. 10, no. 5, p. 100, 2024. doi:10.3390/jimaging10050100
[14] J. Yang, X. Sun, and S. Teng, "Automatic road crack detection using CNN based on semi-supervised learning," *Engineering and Applied Sciences*, vol. 9, no. 4, pp. 85–92, 2024. doi:10.11648/j.eas.20240904.13
[15] J. Yang, X. Sun, and S. Teng, "Automatic road crack detection using CNN based on semi-supervised learning," *Engineering and Applied Sciences*, vol. 9, no. 4, pp. 85–92, 2024. doi:10.11648/j.eas.20240904.13
[16] G. Zhu, S. L. Shen, J. Yao, M. Wang, J. Zhuang, and Z. Fan, "Automatic lightweight networks for real-time road crack detection with DPSO," *Advanced Engineering Informatics*, vol. 68, p. 103610, 2025. doi:10.1016/j.aei.2025.103610
[17] K. Zeng, R. Fan, and X. Tang, "Efficient and accurate road crack detection technology based on YOLOv8-ES," *Autonomous Intelligent Systems*, vol. 5, no. 1, p. 4, 2025. doi:10.1007/s43684-025-00091-3
[18] Y. Yin, J. Yu, P. Chen, J. Chen, X. Ma, and Z. Dong, "Road crack detection of drone-captured images based on TPH-YOLOv5," *Int. J. Pavement Engineering*, vol. 26, no. 1, 2025. doi:10.1080/10298436.2025.2474729
[19] X. Li, Y. Chu, T. Chan, W. L. Lo, and H. Fu, "YOLO-ERCD: An upgraded YOLO framework for efficient road crack detection," *Sensors*, vol. 26, no. 2, p. 564, 2026. doi:10.3390/s26020564
[20] D. Wang, X. Huang, W. Xu, J. Lin, and Y. Zhou, "Lightweight multi-scale feature fusion algorithm for mountain road crack detection," *Signal, Image and Video Processing*, vol. 20, no. 2, p. 52, 2026. doi:10.1007/s11760-026-05123-w
[21] A. Naseri, A. Golroo, and A. Parsaei, "Comparison of different deep learning algorithms in pave- ment crack detection," *Road Materials and Pavement Design*, vol. 27, no. 3, pp. 900–917, 2026. doi:10.1080/14680629.2025.2498107
[22] B. Song, *Topics in Variational PDE Image Segmentation, Inpainting and Denoising*. PhD thesis, University of California, Los Angeles, 2003.
[23] P. Karasev *et al.*, "Interactive medical image segmentation using PDE control of active contours," *IEEE Trans. Medical Imaging*, vol. 32, no. 11, pp. 2127–2139, 2013.
[24] M. Raissi, P. Perdikaris, and G. E. Karniadakis, "Physics-informed neural networks: A deep learning framework for solving forward and inverse problems involving nonlinear partial differential equations," *J. Computational Physics*, vol. 378, pp. 686–707, 2019. doi:10.1016/j.jcp.2018.10.045
[25] A. Zinihi, M. R. S. Ammi, and A. Bachir, "Multi-city modeling of epidemics using a topology- based SIR model: Neural network-enhanced SAIRD model," *J. Computational Science*, p. 102721, 2025. doi:10.1016/j.jocs.2025.102721
[26] R. A. Adams and J. J. Fournier, *Sobolev Spaces*, vol. 140. Elsevier, 2003.
[27] L. Evans, *Partial Differential Equations*, Graduate Studies in Mathematics. AMS, 2010. doi:10.1090/gsm/019
[28] H. Brezis, *Functional Analysis, Sobolev Spaces and Partial Differential Equations*. Springer, 2011. doi:10.1007/978- 0-387-70914-7
[29] J. L. Lions, *Quelques Me ́thodes de Re ́solution des Proble`mes aux Limites Non-Line ́aires*. Dunod, 1969.
[30] R. Temam, *Navier-Stokes Equations: Theory and Numerical Analysis*. North-Holland, 1977.
[31] H. Brezis, *Functional Analysis, Sobolev Spaces and Partial Differential Equations*, vol. 2. Springer, 2011.
[32] E. Zeidler, *Nonlinear Functional Analysis and Its Applications*. Springer, 1990. doi:10.1007/978-1-4612-0985-0
[33] J. P. Aubin, "Un the ́ore`me de compacite ́," *C R Acad Sci Paris*, vol. 256, pp. 5042–5044, 1963.
[34] A. Zinihi, M. R. S. Ammi, and D. F. Torres, "Fractional differential equations of a reaction-diffusion SIR model," *Evolution Equations and Control Theory*, vol. 14, no. 5, pp. 944–967, 2025. doi:10.3934/eect.2025018
[35] EdmCrack600: A pixel-level annotated dataset for crack identification. [Online]. Available: https://github.com/mqp2259/EdmCrack600
[36] O. Ronneberger, P. Fischer, and T. Brox, "U-Net: Convolutional networks for biomedical image segmentation" in *Lecture Notes in Computer Science*, pp. 234–241, Springer, 2015. doi:10.1007/978-3-319-24574-4 28
[37] O. Oktay *et al.*, "Attention U-Net: Learning where to look for the pancreas," arXiv:1804.03999, 2018. doi:10.48550/ARXIV.1804.03999
[38] S. Bai, L. Yang, Y. Liu, and H. Yu, "DMF-Net: A dual-encoding multi-scale fusion network for pavement crack detection," *IEEE Trans. ITS*, vol. 25, no. 6, pp. 5981–5996, 2024. doi:10.1109/tits.2023.3331769
[39] J. Chen *et al.*, "TransUNet: Transformers make strong encoders for medical image segmentation," arXiv:2102.04306, 2021. doi:10.48550/ARXIV.2102.04306
[40] T. F. Chan and L. A. Vese, "Active contours without edges," *IEEE Trans. Image Processing*, vol. 10, no. 2, pp. 266–277, 2001. doi:10.1109/83.902291
[41] S. Osher, R. Fedkiw, and K. Piechor, "Level set methods and dynamic implicit surfaces," *Appl. Mech. Rev.*, vol. 57, no. 3, pp. B15–B15, 2004. doi:10.1115/1.1760521
[42] T. Chan, A. Marquina, and P. Mulet, "High-order total variation-based image restoration," *SIAM J. Scientific Com- puting*, vol. 22, no. 2, pp. 503–516, 2000. doi:10.1137/S1064827598344169
[43] C. Li, C. Xu, C. Gui, and M. D. Fox, "Distance regularized level set evolution and its application to image segmen- tation," *IEEE Trans. Image Processing*, vol. 19, no. 12, pp. 3243–3254, 2010. doi:10.1109/TIP.2010.2069690
[44] V. Caselles, R. Kimmel, and G. Sapiro, "Geodesic active contours," *Int. J. Computer Vision*, vol. 22, pp. 61–79, 1997. doi:10.1023/A:1007979827043

Authors' Profiles



Omar Knnou is a researcher in the MSIA Team at the IMIA Laboratory, Faculty of Sciences and Technics, Errachidia, University of Moulay Ismail, Morocco. His research focuses on computer vision, image segmentation, data science, and artificial intelligence applications.



Rachid Benoudi is a researcher in the MSIA Team at the IMIA Laboratory, Faculty of Sciences and Technics, Errachidia, University of Moulay Ismail, Morocco. His research focuses on computer vision, image segmentation, and deep learning applications.



Mourad Haddioui is a researcher in the MSIA Team at the IMIA Laboratory, Faculty of Sciences and Technics, Errachidia, University of Moulay Ismail, Morocco. His research interests include mathematical modeling, neural networks, and intelligent systems.



Said Agoujil received the M.S. and Ph.D.degrees in mathematics from the Faculty of Sciences and Technology of Marrakech (FSTM), Morocco, in 2004 and 2008, respectively. He is currently a Professor with the Department of Computer Science, ENCG, Moulay Ismail University, EL Hajeb, Morocco. His current research interests include numerical analysis, wireless networks, linear algebra, and speech coding.



Youssef Qaraai is a Professor at Moulay Ismail University Meknes Morocco, specializing in the fields of applied mathematics and computer science. He obtained his PhD in applied mathematics, specializing in Analysis and Control of Systems, in 2008. His research interests include numerical analysis, scientific computing, and differential equations.

How to cite this paper:

Omar Knnou, Rachid Benoudi, Mourad Haddioui, Said Agoujil, Youssef Qaraai, "Efficient Road Cracks Segmentation Using Physics Informed Neural Network Approach", International Journal of Image, Graphics and Signal Processing(IJIGSP), Vol.18, No.3, pp. 54-70, 2026. DOI:10.5815/ijigsp.2026.03.03